Clim Dyn (2016) 46:1753–1768
DOI 10.1007/s00382-015-2672-4

Spatial distribution and the interdecadal change of leading modes of heat budget of the mixed-layer in the tropical Pacific and the association with ENSO

Zeng-Zhen Hu[1] · Arun Kumar[1] · Bohua Huang[2,3]

Received: 15 December 2014 / Accepted: 18 May 2015 / Published online: 29 May 2015

Abstract Using heat budget diagnosis of ocean mixed layer from the Global Ocean Data Assimilation System, the spatial distribution of the leading modes of the heat budget was examined. The analysis was for the tropical Pacific in 1979–2013 and was based on combined empirical orthogonal function (CEOF) analysis. The interdecadal changes of the leading modes and their associations with El Niño-Southern Oscillation (ENSO) were also analyzed. The first leading CEOF mode (CEOF1) corresponds to the ENSO mature phase. The contribution from the zonal advection was relatively small along the equator, except the region near the Pacific coast of Central America. The vertical entrainment and diffusion (surface heat flux) had pronounced maxima with positive (negative) values along the equatorial central and eastern Pacific. The meridional advection displayed a different spatial pattern with large positive values on both sides of the equator and smaller values along the equator. The total meridional advection anomaly was mainly determined by advection of anomalous temperature by climatological current responsible for broadening of the ENSO SSTA pattern meridionally. The zonal advection varied almost simultaneously with the tendency of ocean temperature anomaly in the mixed layer. The second leading CEOF mode (CEOF2) included contribution to SSTA tendency during the ENSO developing phase. The distribution pattern and amplitude of the zonal advection in the eastern Pacific in CEOF2 was similar to but with opposite sign to that in CEOF1. The amplitudes of the other dynamical and thermodynamical terms were smaller than that in CEOF1 and spatial distributions displayed an opposite variation between the Pacific coast of Central America and central and eastern tropical Pacific in CEOF2. A comparison of two periods (1979–1999 and 2000–2013) suggested that coupling in the tropical Pacific weakened at ENSO time scales and shifted to a relatively higher frequency regime (from 2 to 4 years averaged in 1979–1999 to 1.5–3 years) after 2000.

Keywords Spatial distribution · Leading modes of heat budget of the mixed-layer · The tropical Pacific · The association with ENSO · Interdecadal change · Global Ocean Data Assimilation System

✉ Zeng-Zhen Hu
Zeng-Zhen.Hu@noaa.gov

[1] Climate Prediction Center, NCEP/NWS/NOAA, 5830 University Research Court, College Park, MD 20740, USA

[2] Department of Atmospheric, Oceanic, and Earth Sciences, College of Science, George Mason University, 4400 University Drive, Fairfax, VA 22030, USA

[3] Center for Ocean-Land-Atmosphere Studies, 270 Research Hall, Mail Stop 6C5, George Mason University, 4400 University Drive, Fairfax, VA 22030, USA

1 Introduction

El Niño-Southern Oscillation (ENSO) is an ocean–atmosphere coupled phenomenon in the tropical Pacific Ocean, and has significant impacts on global weather and climate variability (e.g., Glantz 2000). ENSO is also the dominant source of predictability of global climate on interseasonal to interannual time scales (e.g., National Research Council 2010). The atmospheric component of ENSO (i.e., the Southern Oscillation) was found almost a century ago by Walker (1923), and near half century later it was found that ENSO is in fact an ocean–atmosphere coupled phenomenon (e.g., Bjerknes 1969). Later, it was further demonstrated that ENSO is not only involved in changes of

surface trade wind and sea surface temperature (SST), but also manifested as changes in the sub-surface ocean variability (e.g., Wyrtki 1975, 1985; Zhang and Levitus 1996; Meinen and McPhaden 2000; Clarke 2010; Kumar and Hu 2014). Indeed, sub-surface ocean changes provide the memory and mechanism for the ENSO transitions from one phase to another, i.e., from El Niño to La Niña and vice versa (Battisti and Hirst 1989; Schopf and Suarez 1987; Jin 1997a, b; Wang 2001). The knowledge of ENSO mechanism provided the physical basis for successful ENSO prediction (Zebiak and Cane 1987).

Due to the importance of sub-surface ocean variation in ENSO evolution and prediction, considerable efforts have focused on the analysis of sub-surface ocean variability. One approach is to examine the heat budget in the ocean mixed layer in the tropical Pacific, which directly connects SST fluctuations with the sub-surface oceanic variations (e.g., Lau et al. 1992; Huang and Schneider 1995; Kang et al. 2001; Zhang et al. 2007; Huang et al. 2010, 2012). For example, Lau et al. (1992) noted a near-balance between horizontal and vertical temperature advection by the time-mean flow, vertical diffusion, and heat input from the overlying atmosphere, while the contributions of transient effects to the balance were negligible. Huang and Schneider (1995) argued that El Niño development is mainly due to advection of anomalous zonal current in the western, the meridional advection in the central, and the displacement of the thermocline in the eastern Pacific. Through analyzing coupled model simulations, Zhang et al. (2007) reported that during ENSO evolution the net surface heat flux acts as a damping mechanism for the mixed-layer ocean temperature anomalies (OTAs), while positive contribution from the advection is dominated by the linear advective process. They further pointed out that the advective feedback by anomalous zonal current and thermocline feedback between SST and OTA are the primary sources responsible for the ENSO phase transition. Huang et al. (2010) diagnosed the heat budget in the ocean mixed layer from the Global Ocean Data Assimilation System (GODAS) and examined its connection with ENSO evolution. They suggested that zonal and meridional temperature advection and vertical entrainment/diffusion all contribute to the onset of an ENSO event and zonal advection plays a dominant role during the decay of the event. The net surface heat flux acted as a damping during the development stage, but played a critical role in the decay of El Niño and the transition to following La Niña. Overall, these previous works suggest that contributions of different thermodynamical and dynamical processes largely depend on ENSO phase as well as the geographical location in the tropical Pacific.

Most of these previous works examined the heat budget terms along the equator or in the Niño regions (such as Niño3.4 region), and their connection with ENSO. However, it is obviously necessary to identify the spatial patterns of each physical process/term associated with ENSO evolution. This is one of the foci of this work. Furthermore, it has been documented that there is an interdecadal transition of the ENSO characteristics around 1999/2000 (e.g., McPhaden 2012; Hu et al. 2013a; Xiang et al. 2013; Kumar and Hu 2014). For example, McPhaden (2012) reported that warm water volume (WWV) integrated along the equatorial Pacific led ENSO SST anomalies (SSTAs) by 2–3 seasons during the 1980/90 s, whereas the variability in WWV, and relationship with ENSO weakened after the 2000s. Hu et al. (2013a) documented a coherent weakening of the interannual variability of the ocean–atmosphere system and linked it with a change of the mean state in the tropical Pacific during 2000–2011. For instance, the equatorial thermocline slope was steeper (flatter) during 2000–2011 (1979–1999), and coincided with positive (negative) SSTAs, increased (decreased) precipitation, and enhanced (suppressed) convection in the western (central and eastern) tropical Pacific, which reflected an intensification of the Walker circulation. Hu et al. (2013a) further argued that the combination of a steeper mean thermocline slope with stronger surface trade winds hampers the eastward migration of the warm water along the equatorial Pacific, resulting in the suppressed ENSO variability. Thus, it is also an interesting research area to compare the spatial distributions of each physical process/term in the heat budget of ocean mixed layer before and after 1999/2000, and to explore their connection with the interdecadal variations of ENSO feature.

In this work, we will focus on the following questions: (1) what are the spatial distributions of leading modes of the dynamical and thermodynamical terms in the heat budget of mixed layer in the tropical Pacific? And what are their associations with ENSO evolution? (2) Are there any differences for the spatial distribution of these leading modes and their connections with ENSO before and after 1999/2000? The paper is organized as follows. After describing the data and analysis approaches in Sect. 2, the first two leading modes of heat budget terms of mixed layer in the tropical Pacific are identified and their connections with ENSO are examined in Sect. 3. In Sect. 4, by comparing the results of CEOF in two separate periods (1979–1999 and 2000–2013), differences of the spatial distribution of first two leading modes and their association with ENSO are examined. A summary with some discussion is given in Sect. 5.

2 Data and analysis approaches

The main dataset used in this work is the heat budget diagnosis of ocean mixed layer (Huang et al. 2010) from

GODAS (Behringer and Xue 2004; Behringer 2005). Following Huang et al. (2010), the tendency of ocean temperature of the ocean mixed layer is defined as:

$$\frac{\partial T}{\partial t} = Q_u + Q_v + Q_w + Q_{zz} + Q_q + R \quad (1)$$

where, $\partial T/\partial t$ is the tendency of mixed layer ocean temperature. Q_u is zonal advection, Q_v is meridional advection, Q_w is vertical entrainment, Q_{zz} is vertical diffusion, and Q_q is adjusted surface heat flux. The adjusted surface heat flux (Q_q) is the net surface heat flux plus heat flux correction (introduced by a relaxation of model SST to observed SST, Huang et al. 2010) minus the penetrative shortwave radiation (Huang et al. 2010). The sum of all Q terms is referred to as total forcing in this work. R is the residual term, which contains the effect of horizontal heat diffusion and the contributions of the sub-monthly processes.

GODAS is an operational oceanic reanalysis at NCEP (Behringer and Xue 2004; Behringer 2005). The ocean model is based on the Geophysical Fluid Dynamics Laboratory Modular Ocean Model version 3 (MOM3), which provides the first guess fields for analysis and is forced with atmospheric fluxes from the NCEP/Department of Energy reanalysis (R2, Kanamitsu et al. 2002). The spatial resolution of MOM3 is 1° (1⁄3°) in zonal (meridional) direction between 10°S and 10°N, gradually increasing through the tropics to 1° poleward of 30°S and 30°N. MOM3 has 40 vertical layers with 27 layers in the upper 400 m of the ocean with a quasi-global (75°S–65°N) configuration. The observational data are assimilated continuously with a four-week data assimilation window through a 3DVAR scheme, and include assimilation of in situ temperature profiles from expendable bathythermographs, Tropical Atmosphere Ocean, Triangle Trans Ocean (TOGA TAO/TRITON) Buoy Network, Pilot Research Moored Array, and Argo profiling floats, as well as SST based on weekly OI SST analysis (Reynolds et al. 2002) (Behringer and Xue 2004; Huang et al. 2010). The reliability of GODAS has been documented for the heat budget diagnosis of ocean mixed layer and its association with ENSO by Huang et al. (2010) and Hu et al. (2012), for the mean state and its variability of ocean temperature along the equator and the connection with interannual and interdecadal variation of ENSO (Kumar and Hu 2014) and tropical Atlantic variability (Hu et al. 2013b).

Surface wind stress from R2, and the depth of 20 °C isotherm (D20), ocean temperature and current from GODAS are used in this analysis. In addition to Niño3.4 index which is the average SSTA in the region (5°N–5°S, 170°W–120°W) (Barnston et al. 1997), WWV index is also used in the analysis. WWV index is defined as average D20 over (120°E–80°W, 5°S–5°N) (Meinen and McPhaden 2000) and is calculated using GODAS data. All data used in this work are monthly mean from Jan 1979–Dec 2013, and anomalies are computed relative to their monthly mean climatologies averaged over respective data periods.

To identify the spatial distribution of leading modes of dynamical and thermodynamical terms of the heat budget of ocean mixed layer in the tropical Pacific, combined empirical orthogonal function (CEOF) analysis is conducted with covariance matrix of six terms: $\partial T/\partial t$ (total forcing), Q_u (zonal advection), Q_v (meridional advection), $Q_w + Q_{zz}$ (vertical entrainment and diffusion), Q_q (adjusted surface heat flux), as well as observed SSTA tendency. The domain is (15°S–15°N, 135.5°E–74.5°W), and latitude (area) weighting is included in the CEOF computation (North et al. 1982). It is expected that, by applying CEOF, we can isolate the physically coherent modes of the heat budget terms and, meanwhile, eliminate the influence of some biases in the heat budget data. In this analysis, we focus on the first two leading modes of CEOF, since the higher modes explain much smaller fraction of the total variance and are not easy to be interpreted physically.

The connections of the leading spatial modes with ENSO evolution are examined by computing the lead-lag correlations of the corresponding principle components (PCs) with Niño3.4 and WWV indices, as well as regressions of surface wind stress, SST and D20 onto the PCs. Furthermore, in addition to the CEOF analysis for the whole period (Jan 1979–Dec 2013), CEOF analyses are also calculated for two separated periods (Jan 1979–Dec 1999 and Jan 2000–Dec 2013), as well as a wavelet analysis of Niño3.4 index is conducted to explore the interdecadal changes of ENSO feature (spatial patterns of the leading modes of heat budget terms and ENSO period) that went through a dramatic change around 1999/2000 (e.g., McPhaden 2012; Hu et al. 2013a; Xiang et al. 2013; Kumar and Hu 2014).

3 Leading modes and their connection with ENSO

3.1 CEOF1

Figure 1 shows the time series (PC1) and the corresponding patterns of first leading CEOF mode (CEOF1). From the lead-lag correlation between PC1 and Niño3.4 index (bars in Fig. 2a), we note that the maximum correlation presents when they are simultaneous. For the lead-lag correlations of PC1 with WWV index (bars in Fig. 2b), the maximum correlation occurs when WWV index leads PC1 by 1–2 months, implying that this mode is connected with a reduced tendency of positive (negative) anomaly of total heat content in the mixed layer along the equatorial Pacific and the discharge (recharge) process (Jin 1997a, b; Meinen and McPhaden 2000; Kumar and Hu 2014). These

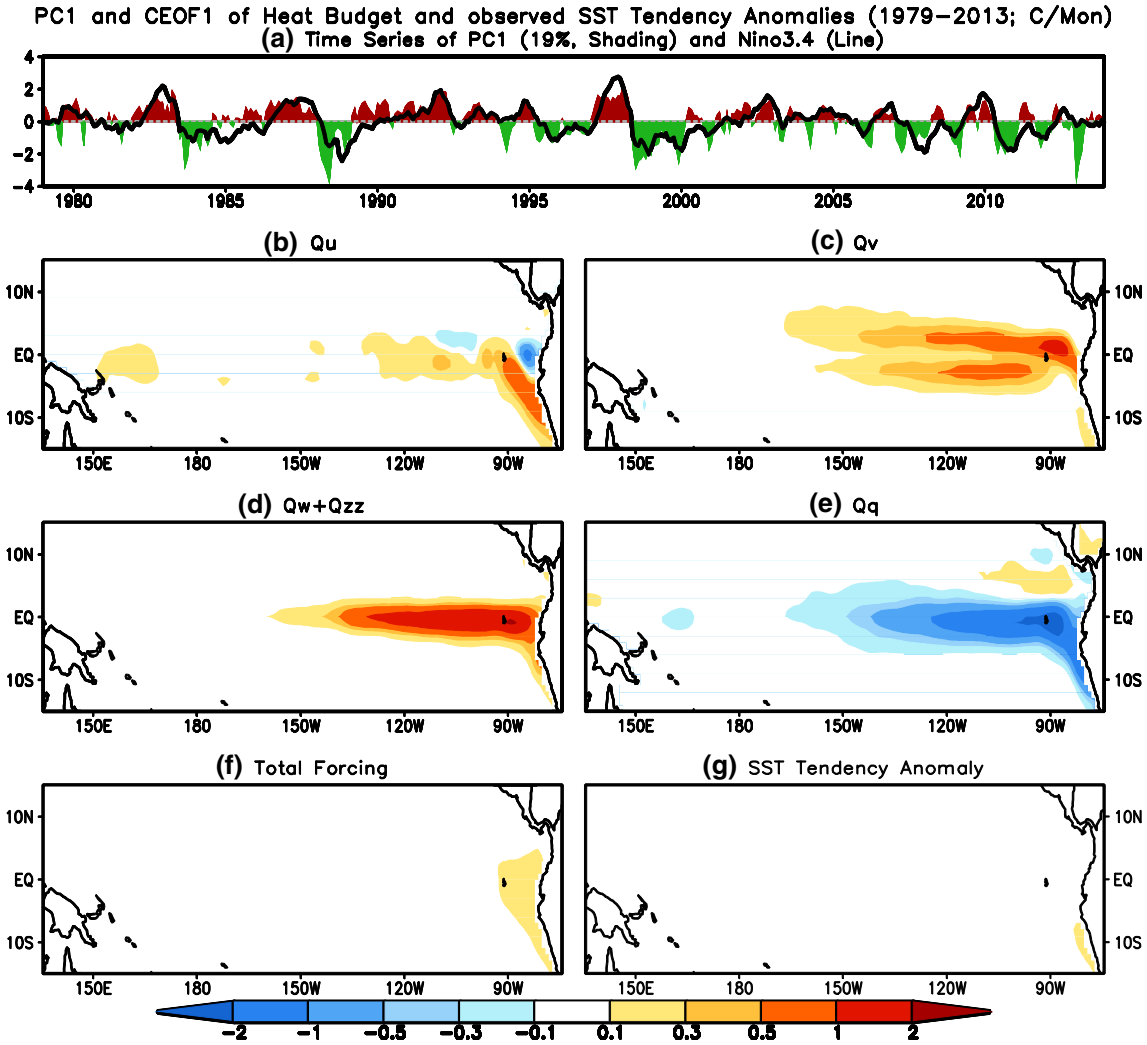

Fig. 1 **a** PC1 (*shading*), and CEOF1 of **b** Q_u, **c** Q_v, **d** Q_w+Q_{zz}, **e** Q_q, **f** total forcing, and **g** SSTA tendency. *Curve* in **a** is the time series of Niño3.4 index. This mode explains 19 % of the total variance

results suggest that CEOF1 corresponds to heat budget terms in the ENSO peak phase. This is also consistent with small value for total forcing (Fig. 1f) and SSTA tendency (Fig. 1g), as well as the regressions of the contemporaneous SST and surface wind stress anomalies onto PC1 (Fig. 3e). The lead-lag regressions (Fig. 3) display a typical SST and surface wind stress anomaly evolution associated with ENSO cycle (Rasmusson and Carpenter 1982; Sarachik and Cane 2010).

In the ENSO mature phase, the contribution from the zonal advection (Q_u) is relatively small in the tropics, except the region near the Pacific coast of Central America with a structure reminiscent of the equatorward extension of the cold tongue (Fig. 1b). It seems to suggest that, with weaker coastal upwelling, the westward advection of the cold water is also weakened. The values of the vertical entrainment and diffusion ($Q_w + Q_{zz}$), and the adjusted surface heat flux (Q_q) are pronounced with positive maxima for the former and negative maxima for the latter along the equatorial central and eastern Pacific (Fig. 1d, e). This implies that the vertical entrainment and diffusion increases the OTA in the mixed layer while the adjusted surface heat flux acts to damp ENSO SSTA. The small total forcing (Fig. 1f) implies that the dynamical and thermodynamical processes balance each other in the mature phase of ENSO, though each term on its own has large spatial loading. The EOF result also shows that the residual term (R) is negligible in most of the places (not shown), except for the eastern coastal region. Although the residual term may be small if compared with individual dynamical and thermodynamical terms, but may not be small if compared with tendency or total forcing term, resulting in unbalanced heat budgets. It is expected that through the EOF analysis, we can exclude the unbalance

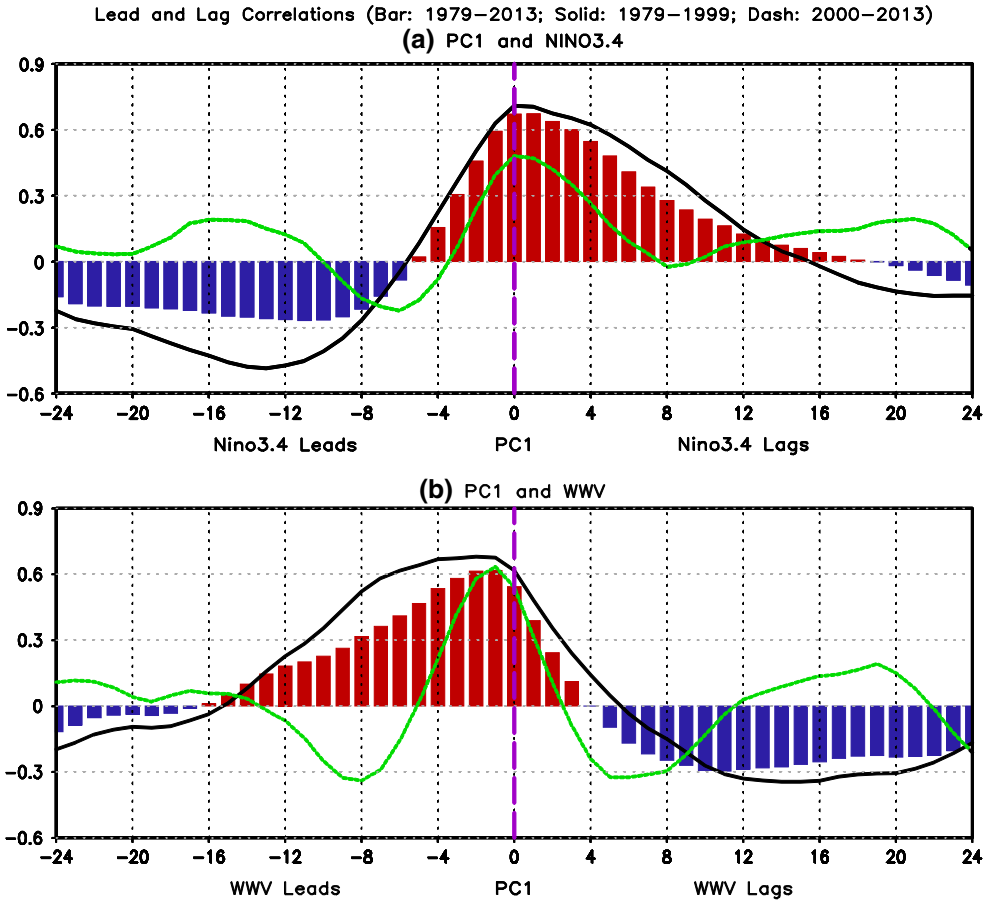

Fig. 2 Lead and lag correlations between **a** PC1 and Niño3.4 index, **b** PC1 and WWV index. *Bar* is the correlations with PC1 in Jan 1979/80–Dec 2013 (*shading* in Fig. 1a), *solid/black line* with PC1 in Jan 1979/80–Dec 1999 (see *shading* in Fig. 9a), and *dash/green line* with PC1 in Jan 2000–Dec 2013 (see *bars* in Fig. 9a)

potion and identify the physical consistent leading pattern associated with ENSO.

The meridional advection (Q_v) displays a spatial pattern with large positive values on the two sides of the equator. Further analysis shows that the regression (correlation) pattern of oceanic meridional heat advection onto normalized Niño3.4 index is similar to that onto normalized PC1 (left and right panels, Fig. 4a), suggesting a direct connection of the oceanic meridional heat advection with ENSO, as well as the importance of the oceanic meridional heat advection in ENSO evolution. Here we should point out that the calculations shown in Fig. 4 were done by averaging above a constant depth of 55 m using data from GODAS. Although this average is different from average over the mixed layer, particularly for the western tropical Pacific with deeper mixed layer (see Fig. 1c, d of Kumar and Hu 2014), the 55 m depth is on the same order as the mixed layer depth in the central and eastern equatorial Pacific. It seems that the difference in averaging depth should not change the general conclusion.

Among the different components of the anomalous oceanic meridional heat advection, advection of anomalous ocean temperature by climatological meridional ocean current plays a dominant role (Fig. 4b), while advection of both anomalous and climatological ocean temperature by anomalous current makes little contribution (Fig. 4c, d). Nevertheless, the spatial distribution of CEOF1 of Q_v on two sides of the equator is symmetric to the equator (Fig. 1c), while the regression and correlation pattern has amplitude asymmetry across the equator, particularly in the eastern Pacific (eastward of 120°W). Also, the signal in the central Pacific in the regression and correlation (Fig. 4a, b) is much stronger than that in CEOF1 (Fig. 1c). These differences are probably due to the fact that the depths of the vertical integration are different between the mixed layer heat budget diagnosis and our meridional heat transport analysis. In general, the role of the meridional heat advection is to expand the equatorial SST anomalies, generated in the central and eastern equatorial Pacific by the vertical advections to the south and north. As a result, the equatorial

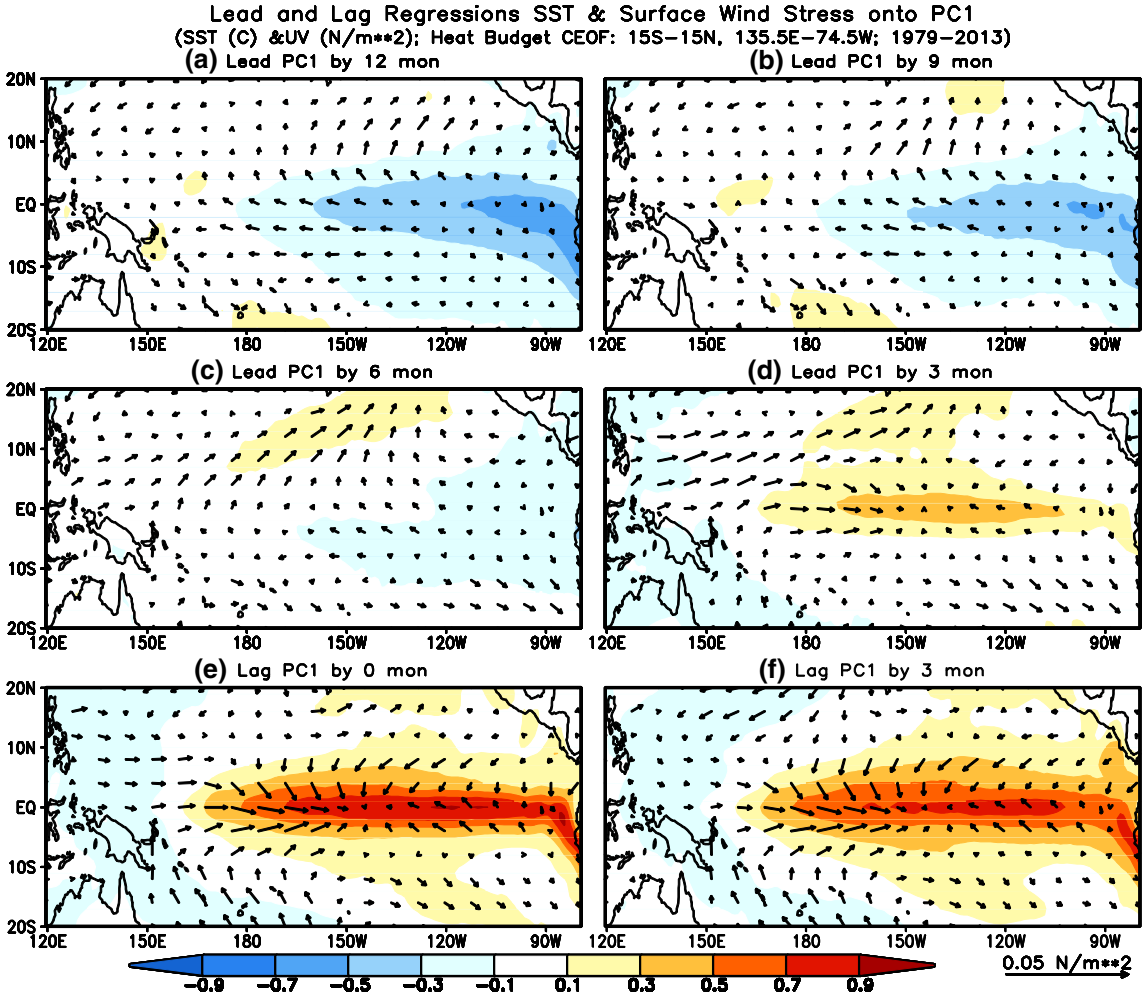

Fig. 3 Lead and lag regressions of surface wind tress (*vectors*) and SST (*shading*) anomalies onto PC1 for leading PC1 by **a** 12 months, **b** 9 months, **c** 6 months, and **d** 3 months, for lagging PC1 by **e** 0 month, and **f** 3 months. The unit is °C per standard deviation of PC1 for the SST regression, and N/m^2 per standard deviation of PC1 for the wind stress regression

SST anomalies (e.g., Fig. 3e) occupy a wider latitude span than the pattern of the vertical advection (Fig. 1d) would imply.

3.2 CEOF2

Figure 5 shows the time series (PC2) and the corresponding patterns of second leading CEOF mode (CEOF2). Compared with the lead-lag correlations between PC2 and Niño3.4 index (bars in Fig. 6a), the correlations between PC2 and WWV index is larger when WWV lags PC2 by 0-3 months (bars in Fig. 6b). The maximum correlations with WWV appear when PC2 leads WWV index by 1–2 months. This suggests that the mode is connected with an enhanced tendency of the total heat content anomaly in the mixed layer along the equatorial Pacific and may be involved in changing the WWV tendency through the meridional recharge/discharge processes (Jin 1997a, b; Meinen and McPhaden 2000; Kumar and Hu 2014). This is also supported by the lead-lag regressions of D20 and surface wind stress anomalies onto PC2 (Fig. 7) as well as the lead-lag regressions of ocean horizontal and vertical current anomalies onto PC2 (not shown). The regressions show positive D20 anomalies along the equatorial Pacific when lagging PC2 by 0–6 months, suggesting an accumulation of ocean heat along the equator. In fact, that is a precursor for El Niño or La Niña occurrence according to the recharge oscillator theory (Jin 1997a, b). The correlations between PC2 and Niño3.4 index changes from positive to negative for Niño3.4 index leading PC2 to lagging PC2 (bars in Fig. 6a). This fact, as well as the positive total forcing and SSTA tendency (Fig. 5f, g), indicate that this mode is associated with the development phase of ENSO.

It is noted that the distribution pattern and amplitude of zonal advection in the eastern Pacific in the ENSO development phase is similar but with opposite sign to that in the ENSO mature phase (Figs. 1b, 5b). Along the equator, zonal

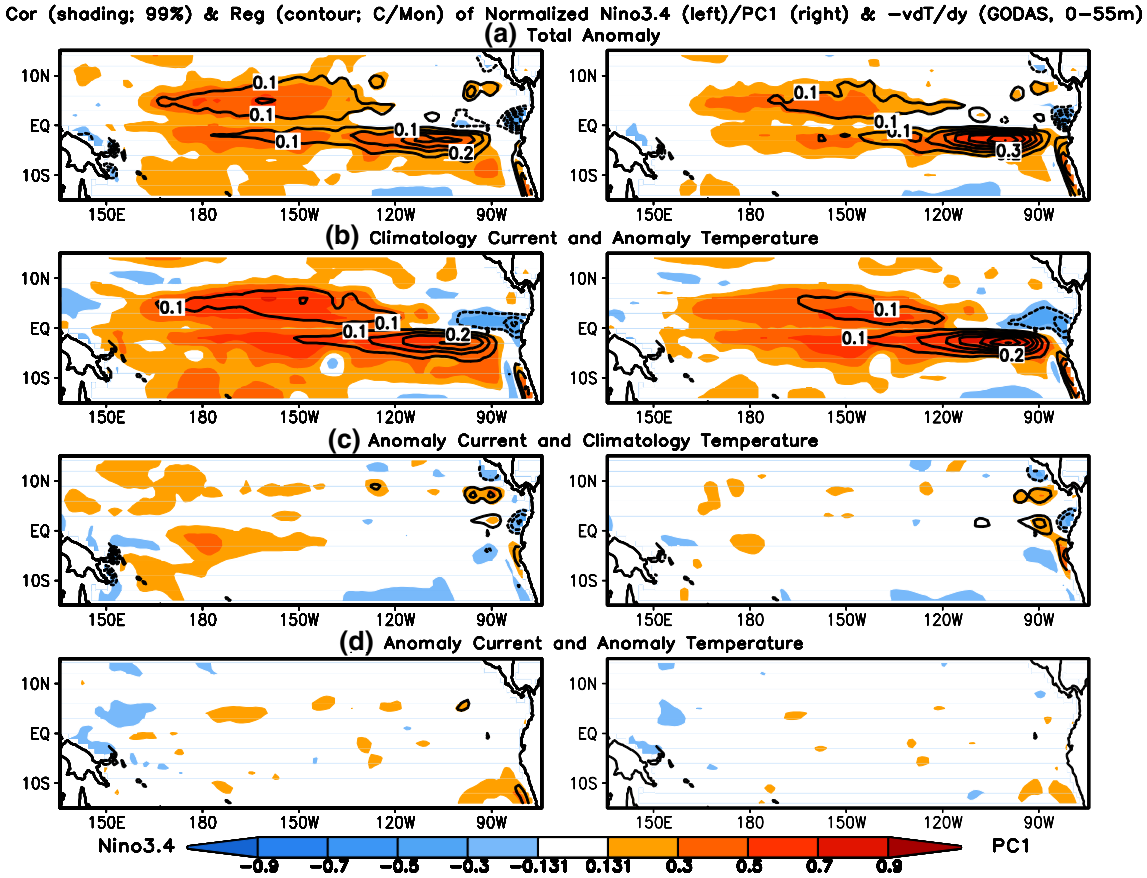

Fig. 4 Regressions of oceanic meridional heat advection averaged between the ocean surface and 55 m depth onto normalized Niño3.4 index (*left column*) and PC1 (*right column*) for **a** total anomalous advection, for the anomalous advection component caused by **b** climatology current and anomaly temperature, **c** anomaly current and climatology temperature, and **d** anomaly current and anomaly temperature. The unit is °C/month per standard deviation of Niño3.4 index (*left panel*) and PC1 (*right panel*) for the regression. The *shading* represents the corresponding correlation at 99 % or higher confidence level using *T* test

advection generates positive tendency from the dateline to 120°W, which is associated with anomalous zonal currents during the initiation of an ENSO event (e.g., Huang and Schneider 1995; Picaut et al. 1997; Kang et al. 2001). The main equatorial warming tendency, however, is generated by the downwelling effect associated with the deepened thermocline depth (Fig. 5d) and broadened by the off-equatorial warming due to meridional heat advection (Fig. 5c).

For the other dynamical and thermodynamical terms, both the distribution pattern and amplitude show clear differences between the ENSO mature and development phases (Figs. 1c–e, 5c–e). For example, the overall amplitudes are smaller in the develop phase than in the ENSO mature phase. Moreover, all spatial distributions display an opposite variation between the Pacific coast of Central America and the central and eastern tropical Pacific. This may imply a zonal extension or propagation along the equator for the contribution of the meridional advection and the vertical entrainment and diffusion processes from the development to the mature phases of ENSO evolution.

4 Interdecadal changes of the leading modes and their connection with ENSO

We noted that amplitudes of both PC1 and PC2 decreased after 1999/2000 (shading in Figs. 1a, 5a). This is consistent with the fact that the variabilities of Niño3.4 and WWV indices (line in Figs. 1a, 5a) were also reduced after 1999/2000. This also agrees with suppression in ENSO variability after 1999/2000 (e.g., McPhaden 2012; Hu et al. 2013a; Xiang et al. 2013; Kumar and Hu 2014). Hu et al. (2013a) argued by diagnosis and model sensitivity experiments that the decrease of ENSO variability is tied with the enhanced east–west contrast in the tropical Pacific. In addition to the variability change, McPhaden (2012) reported a shift of the relationship between ENSO and WWV integrated along the equatorial Pacific around 1999/2000, leading to change in ENSO prediction skill (Wang et al. 2010). McPhaden (2012) found that while WWV led ENSO SST anomalies by 2–3 seasons during the 1980/90s, variability in WWV decreased and lead time was reduced to only one

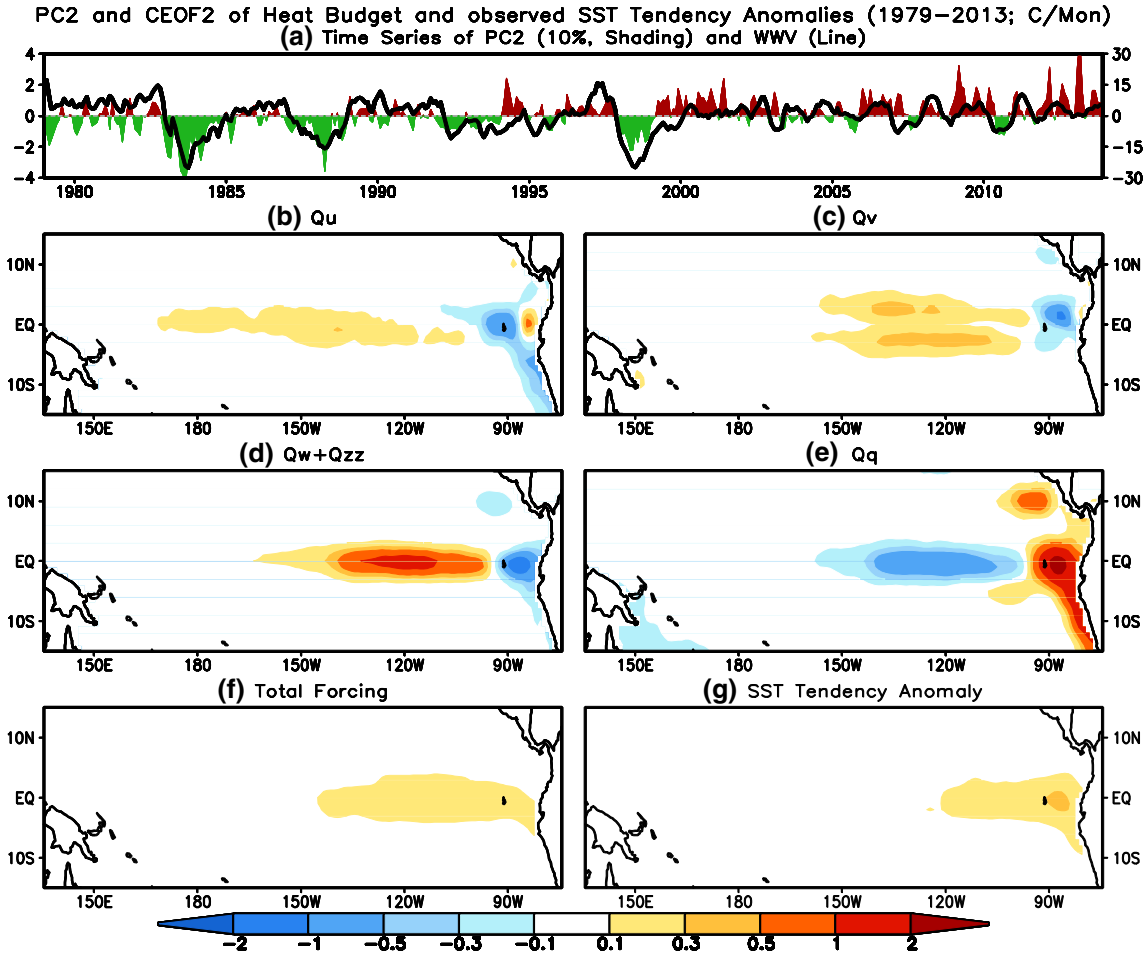

Fig. 5 **a** PC2 (*shading*), and CEOF2 of **b** Q_u, **c** Q_v, **d** Q_w+Q_{zz}, **e** Q_q, **f** total forcing, and **g** SSTA tendency. *Curve* in **a** is the time series of WWV index. This mode explains 10 % of the total variance

season during the 2000s. Recently, Kumar and Hu (2014) also documented that the time scales of PCs of two leading modes of OTA along the equatorial Pacific (called tilt and WWV modes, respectively) and their association with ENSO evolution shortened since 1999/2000 (see their Figs. 2, 6).

Our calculations of CEOF over two separate periods (1979–1999 and 2000–2013) confirm that this is also the case for the heat budget terms in the ocean mixed layer in the tropical Pacific. For example, compared with that in 1979–1999 (solid/black lines in Figs. 2, 6), both the time scales associated with the Niño3.4 and WWV indices for PC1 and PC2 in 2000–2013 became shorter (dashed/green lines in Figs. 2, 6). Furthermore, reduction in ENSO variance and period shortening since 1999/2000 are confirmed by wavelet analysis. To demonstrate this, first we decompose Niño3.4 index into different time scales through wavelet analysis (Hu and Nitta 1996). Then, the variances of wavelet components at different time scales are computed and shown in Fig. 8. From Fig. 8, it is noted that the variances largely reduced since 1999/2000. Meanwhile, the time scales having maximum variance shifted from about 2–4 years for the average in 1979–1999 to about 1.5–3 years for the average in 2000–2013, indicating shortening of the oscillation period of ENSO since 1999/2000. This is also consistent with a recent analysis of Kumar and Hu (2014) based on the examination of the leading modes of OTA along the equatorial Pacific in GODAS and their connections with ENSO evolution as well as their interdecadal variation. Collectively, this may suggest that the coupled system in the tropical Pacific shifted to a relatively higher frequency regime after 2000 compared with that in 1979–1999. We next examine if the spatial patterns of the leading modes of the heat budget terms in the ocean mixed layer associated with ENSO also change and what the changes are.

Figure 9 shows the results of CEOF1 computed over two separate periods (1979–1999 and 2000–2013). We note that both spatial pattern and amplitude of the zonal advection show little change (Fig. 9b). However, the fractions of the

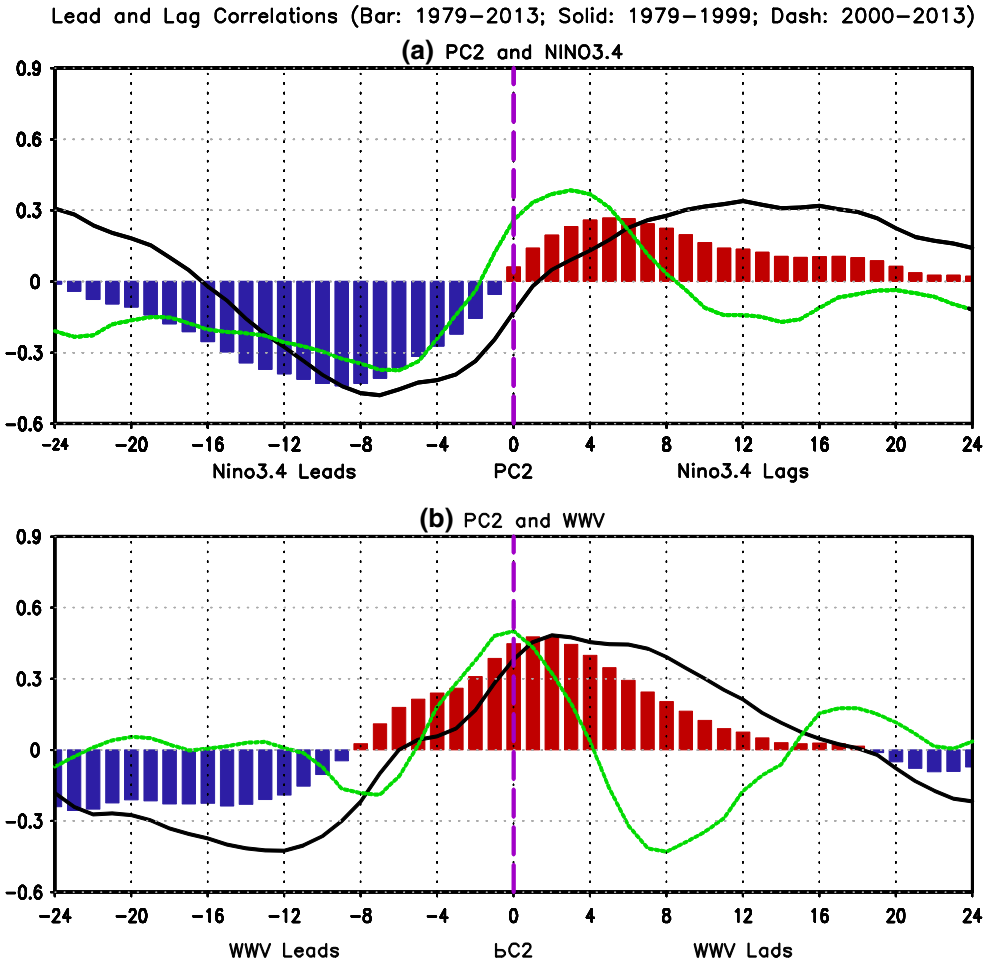

Fig. 6 Lead and lag correlations between **a** PC2 and Niño3.4 index, **b** PC2 and WWV index. *Bar* is the correlations with PC2 in Jan 1979/80–Dec 2013 (*shading* in Fig. 5a), *solid/black line* with PC2 in Jan 1979/80–Dec 1999 (see *shading* in Fig. 10a), and *dash/green line* with PC2 in Jan 2000–Dec 2013 (see *bars* in Fig. 10a)

total variance explained by CEOF1 decreased from 22 % in Jan 1979–Dec 1999 to 16 % in Jan 2000–Dec 2013. Statistically, the ratio of the variances in the two periods is significant at level of 95 % using F-test. Nevertheless, caution is warranted due to the short length of overall data and different length of the two data segments as well as possible impact of the residual term. Also, the amplitudes of meridional advection, vertical entrainment and diffusion and adjusted surface heat flux were smaller in 2000–2013 than in 1979–1999, although the overall patterns were similar (comparing the left and right panels in Fig. 9c–e). The differences of CEOF2 (Fig. 10) between the two segments are less pronounced compared with that of CEOF1. Also, the fractions of the total variance explained by CEOF2 (11 and 10 %) are comparable in the two periods.

Thus, the comparison of CEOF results over the two segments suggests that overall ocean–atmosphere coupling weakened at the ENSO time scales during the ENSO mature phase after 1999/2000 and were similar in the ENSO developing phase. The weakening of coupling at the ENSO time scales indicated by the CEOF analyses is consistent with the variance changes of the different terms as well as SSTA and D20 anomaly between the two periods shown in Fig. 11. The overall variances of all the heat budget terms are larger in the earlier period than in the latter period (Fig. 11a–d). That is in line with the corresponding variance differences of SSTA and D20 anomaly (Fig. 11e, f). Again, the variance changes confirm the weakening of ocean variability at the ENSO time scales in the equatorial Pacific mixed layer since 2000s (McPhaden 2012; Hu et al. 2013a; Kumar and Hu 2014; Wen et al. 2014).

In addition to the weakening in the intensity, the zonal extension of SSTA suggests large variability from the Pacific coast of Central America to the central equatorial Pacific in the earlier period, while in the latter period, there are two maximum variability centers which are in the eastern and central equatorial Pacific, respectively (Fig. 11e). This agrees with the fact that maximum SSTA

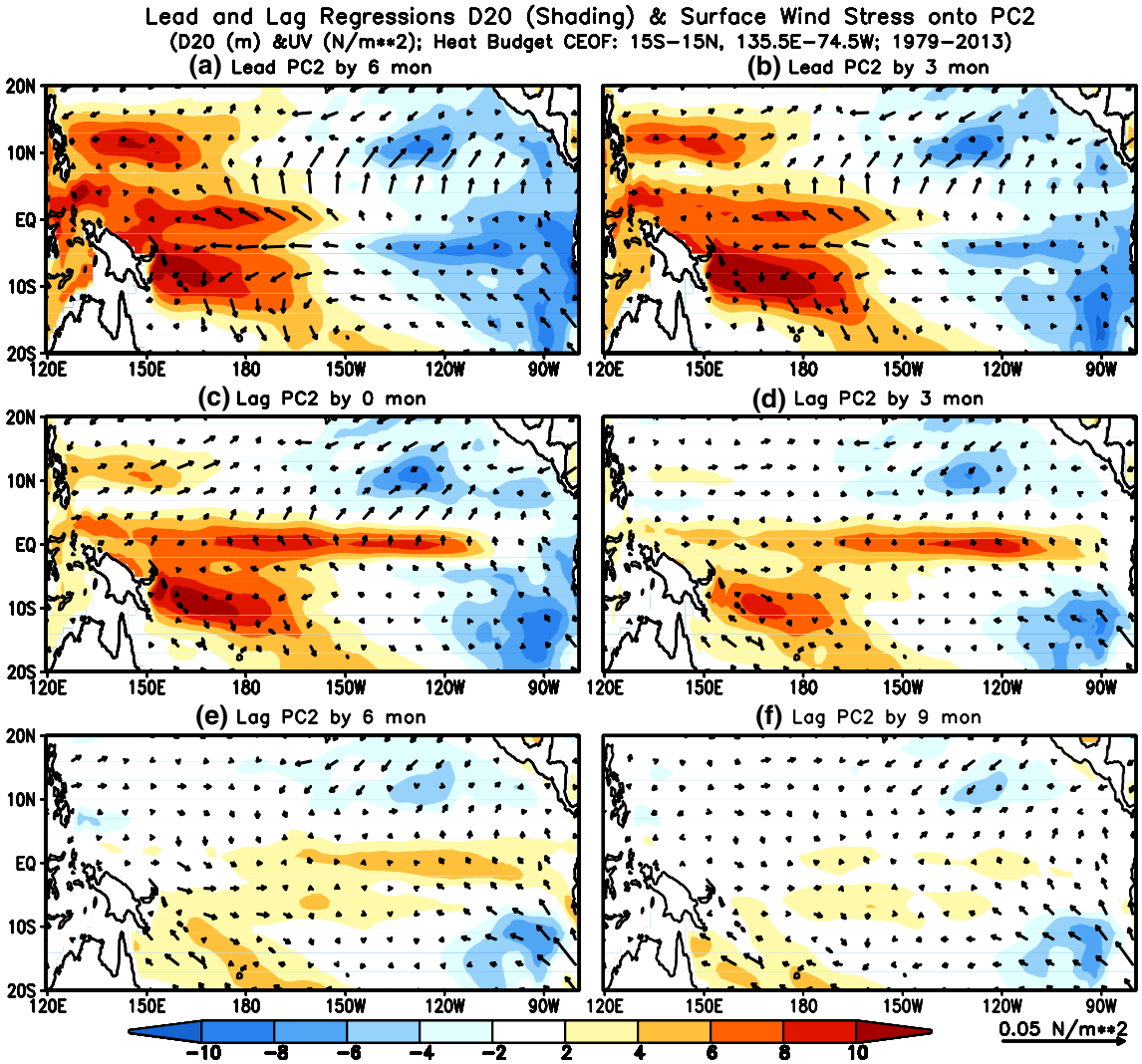

Fig. 7 Lead and lag regressions of surface wind tress (*vectors*) and D20 (*shading*) anomalies onto PC2 for leading PC2 by **a** 6 months, and **b** 3 months, for lagging PC2 by **c** 0 month, **d** 3 months, **e** 6 months, and **f** 9 months. The unit is m per standard deviation of PC2 for the D20 regression, and N/m^2 per standard deviation of PC2 for the wind stress regression

associated with El Niño occurs more often in the central Pacific in the recent decades than the earlier decades (Yeh et al. 2009; Lee and McPhaden 2010; Hu et al. 2012). It is likely that the SST variability redistributed over the tropical Pacific basin, in addition to weakening as a whole, but this conclusion could be influenced by differences in the sampling size between the two segments and the short length of the whole data. Comparing Fig. 11e with Fig. 11f suggests that the maximum SSTA variance center in the central Pacific doesn't have collocated maximum center of D20 anomaly variance. This may be an indicator that the maximum SSTA variance center in the central Pacific is not driven by thermocline feedback. That is consistent with previous works (Kug et al. 2009; Kao and Yu 2009; Hu et al. 2012). They documented that zonal advective feedback (i.e., zonal advection of mean SST by anomalous zonal currents) plays a crucial role for the central Pacific-type El Niño, while thermocline feedback is a key process for the eastern Pacific-type El Niño. Therefore, the heat budget terms in the mixed-layer along the equatorial Pacific mayn't fully account for the zonal extension of SSTA variability in the tropical Pacific.

The weakening of overall ocean–atmosphere coupling at the ENSO time scales since 1999/2000 occurred under the background of mean state changes (Fig. 12). For SST (Fig. 12f), the zonal gradient was increased after 1999/2000. This is consistent with enhanced east–west contrast in the tropical Pacific noted by Hu et al. (2013a). The cooling in the eastern tropical Pacific (110°W to the Pacific coast of Central America) seems contributed by an enhancement of all the dynamical terms (Fig. 12a–c). Strikingly, the cooling caused by $Q_w + Q_{zz}$ (vertical entrainment

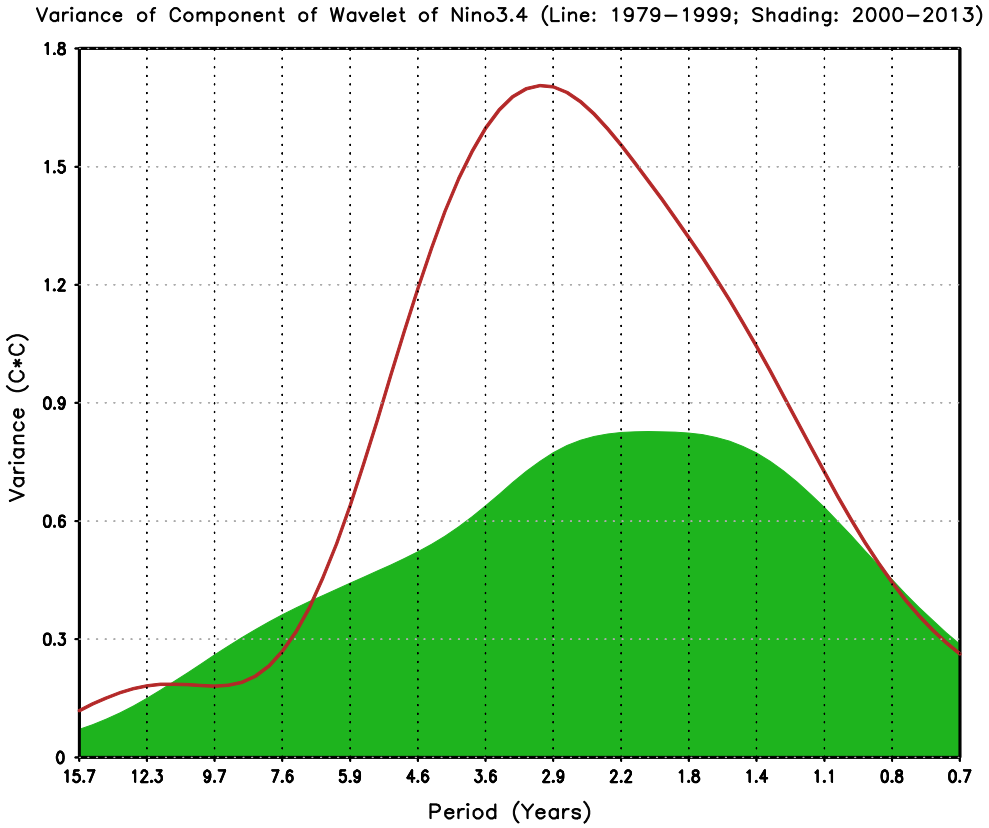

Fig. 8 Variance dependence on time scales of Niño3.4 index for the average in Jan 1979–Dec 1999 (*line*) and in Jan 2000–Dec 2013 (*shading*). See *text* for the details of the calculation

and diffusion, Fig. 12c) weakened between 110°W and 150°W since 1999/2000. The latter suggests that the thermocline feedback in ENSO played a smaller role in this key region of atmosphere–ocean coupling (Barnston et al. 1997). Overall, the dynamical terms are balanced by the thermodynamical terms, resulting in negligible total forcing and its change (Fig. 12a–e).

5 Discussion and conclusions

In this work, using the heat budget diagnosis of ocean mixed layer from the Global Ocean Data Assimilation System, we examined the leading modes of dynamical and thermodynamical terms in the tropical Pacific using combined EOF (CEOF) analysis and their association with ENSO. The interdecadal changes of these leading modes and their associations with ENSO feature change were also analyzed.

The first leading CEOF mode corresponds to spatial patterns of the heat budget terms in the ENSO mature phase. At this stage, the contribution from the zonal advection is relatively small along the equator, except for the region near the Pacific coast of Central America. The vertical entrainment and diffusion, and the adjusted surface heat flux were pronounced with maximum positive values for the former and maximum negative values for the latter along the equatorial central and eastern Pacific. The meridional advection displayed a different spatial pattern with large positive values on both sides of the equator and relatively smaller values along the equator. The total meridional advection anomaly was mainly determined by advection of anomalous temperatures by climatological meridional current and tended to broaden the ENSO SSTA pattern meridionally. It is suggested that the zonal advection varies almost simultaneously with the tendency of OTA in the mixed layer, while the other dynamical and thermodynamical processes are still important, but cancel out in the mature phase of ENSO.

The second leading CEOF mode corresponds to spatial patterns of the heat budget terms in the ENSO development phase. The distribution pattern and amplitude of the zonal advection in the eastern Pacific in the ENSO development phase is similar but with opposite sign to that in the ENSO mature phase. Compared with that in the ENSO mature phase, the amplitudes of the other dynamical and thermodynamical terms are smaller and spatial distributions displayed an opposite variation between the Pacific coast of

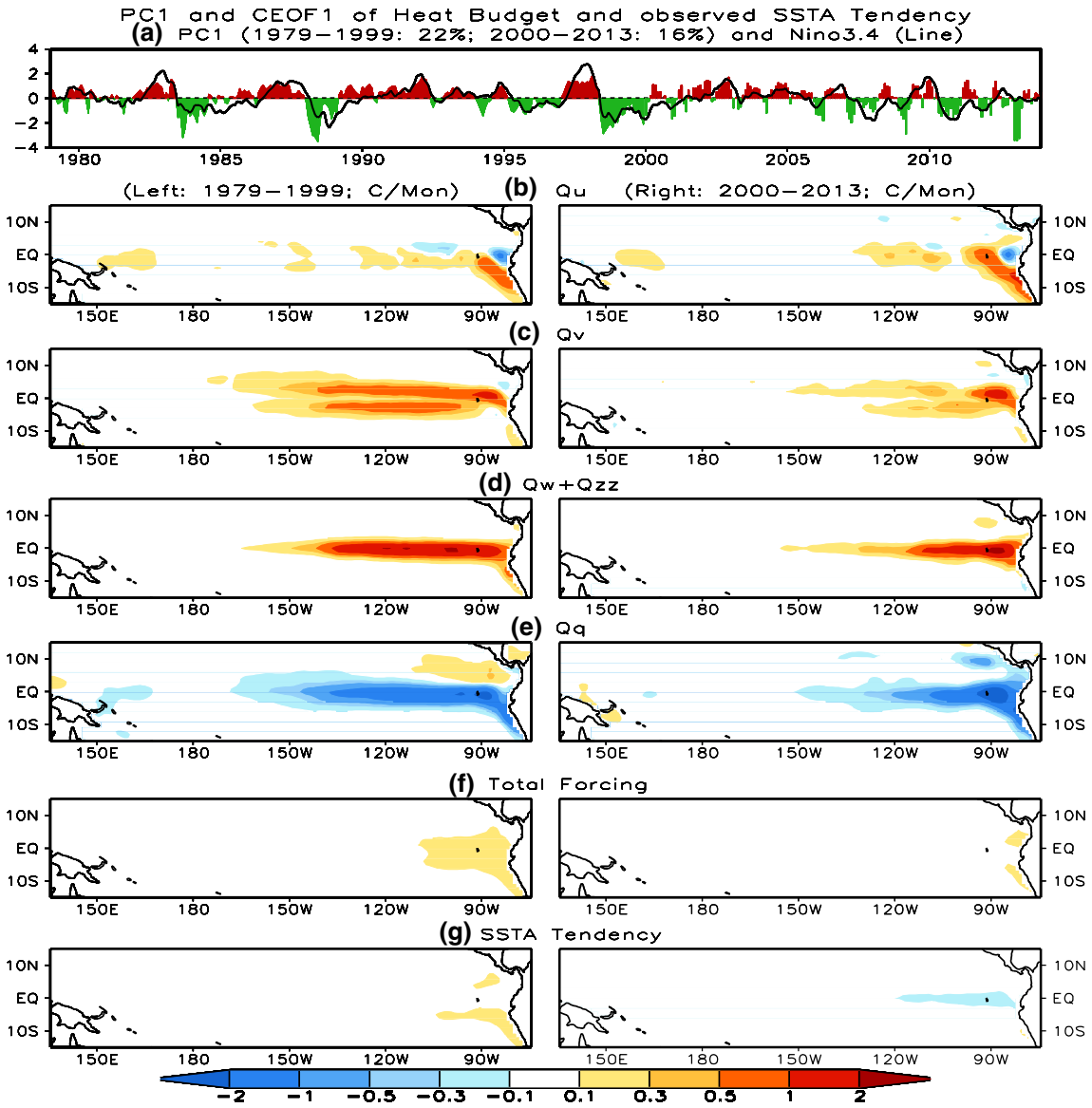

Fig. 9 PC1 and CEOF1 in two separated periods: Jan 1979–Dec 1999 and Jan 2000–Dec 2013. **a** PC1 (*shading* for Jan 1979–Dec 1999 and *bar* for Jan 2000–Dec 2013), and CEOF1 of **b** Q_u, **c** Q_v, **d** Q_w+Q_{zz}, **e** Q_q, **f** total forcing, and **g** SSTA tendency (*left panels* for Jan 1979–Dec 1999 and *right panels* for Jan 2000–Dec 2013). The mode in Jan 1979–Dec 1999 and Jan 2000–Dec 2013 explains 22 and 16 % of the total variance, respectively. *Line* in **a** is the time series of Niño3.4 index

Central America and the central and eastern tropical Pacific in the development phase.

Comparison of CEOF results over the two data periods (1979–1999 and 2000–2013) and their connections with ENSO suggest that amplitudes of both PC1 and PC2 decreased in 2000–2013. Further comparison of the spatial patterns of the corresponding CEOF mode between the two periods suggests that overall coupling weakened at ENSO time scales since 1999/2000. The weakening of the coupling occurred under the climatological background of decreased vertical entrainment and diffusion in the central and eastern equatorial Pacific. In addition, analysis of the zonal extension of SSTA variability suggests large variability from the Pacific coast of Central America to the central equatorial Pacific in the earlier period, while in the latter period, there are two maximum variability centers which are in the eastern and central equatorial Pacific, respectively. It seems that the heat budget terms in the mixed-layer along the equatorial Pacific mayn't fully account for the zonal extension of SSTA variability in the tropical Pacific.

Also, the time scales of both PC1 and PC2 and their associations with Niño3.4 and WWV indices became shorter in 2000–2013 compared with that in 1979–1999.

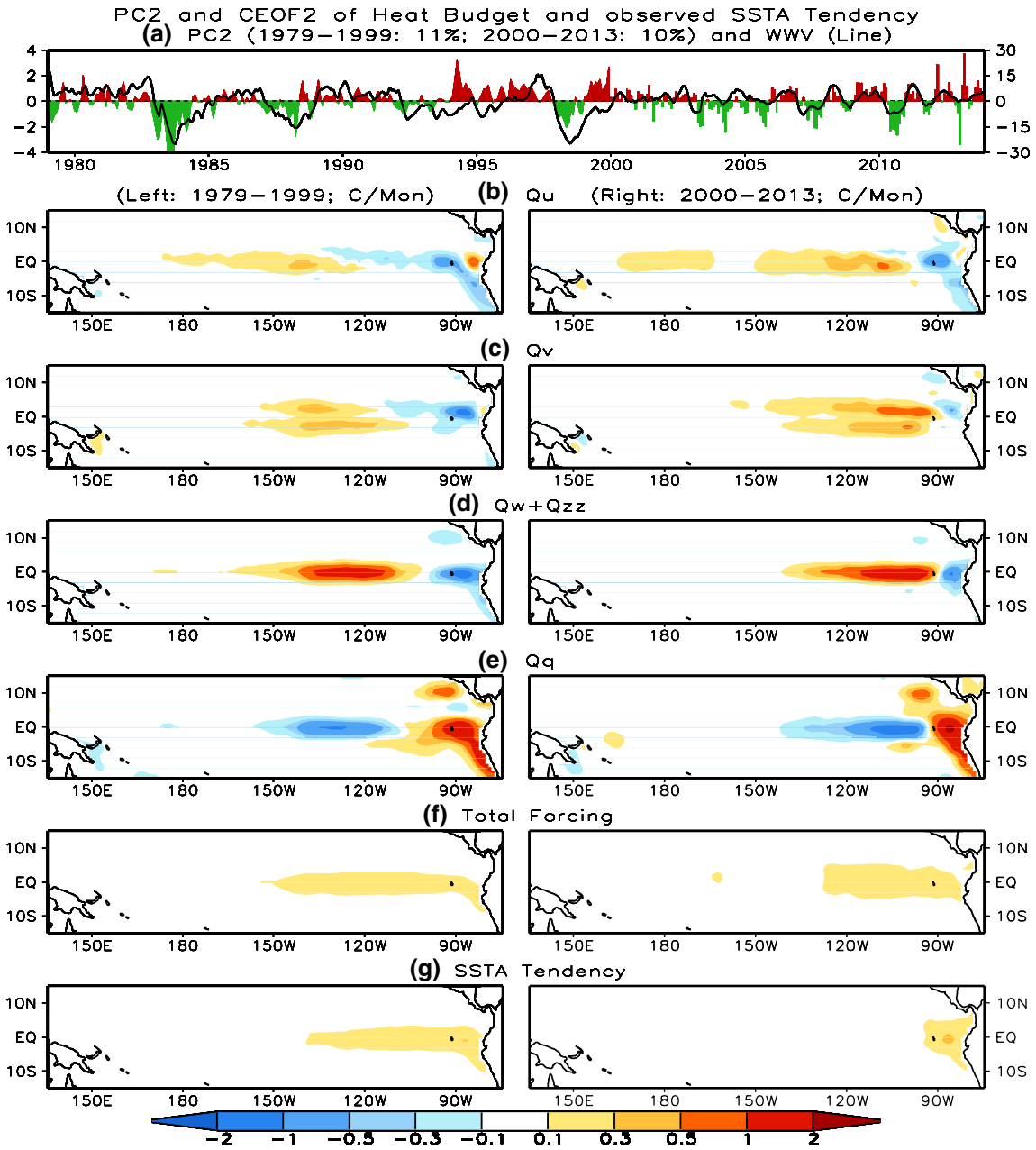

Fig. 10 PC2 and CEOF2 in two separated periods: Jan 1979–Dec 1999 and Jan 2000–Dec 2013. **a** PC2 (*shading* for Jan 1979–Dec 1999 and *bar* for Jan 2000–Dec 2013), and CEOF2 of **b** Q_u, **c** Q_v, **d** Q_w+Q_{zz}, **e** Q_q, **f** total forcing, and **g** SSTA tendency (*left panels* for Jan 1979–Dec 1999 and *right panels* for Jan 2000−Dec 2013). The mode in Jan 1979–Dec 1999 and Jan 2000–Dec 2013 explains 11 and 10 % of the total variance, respectively. *Line* in **a** is the time series of WWV index

Wavelet analysis of Niño3.4 index suggested that dominant period of ENSO variability shifted from 2-4 years averaged in 1979–1999 to 1.5–3 years averaged in 2000–2013. That indicates that the air-sea coupled system in the tropical Pacific shifted to a relatively higher frequency regime after 2000 compared with that in 1979–1999. These results are generally consistent with the observed ENSO amplitude and frequency changes since 2000, which had been documented in previous works (e.g., McPhaden 2012; Hu et al. 2013a; Xiang et al. 2013; Kumar and Hu 2014; Wen et al. 2014).

Clearly, the data are too short, and might affect the robustness of the leading modes discussed in this work (Dommenget and Latif 2002; Bay and Dommenget 2014), particularly for the discussion about the interdecadal variations of the leading modes and their connection with ENSO feature change. Also, these leading modes and their connections with ENSO may vary with season. Lastly, biases

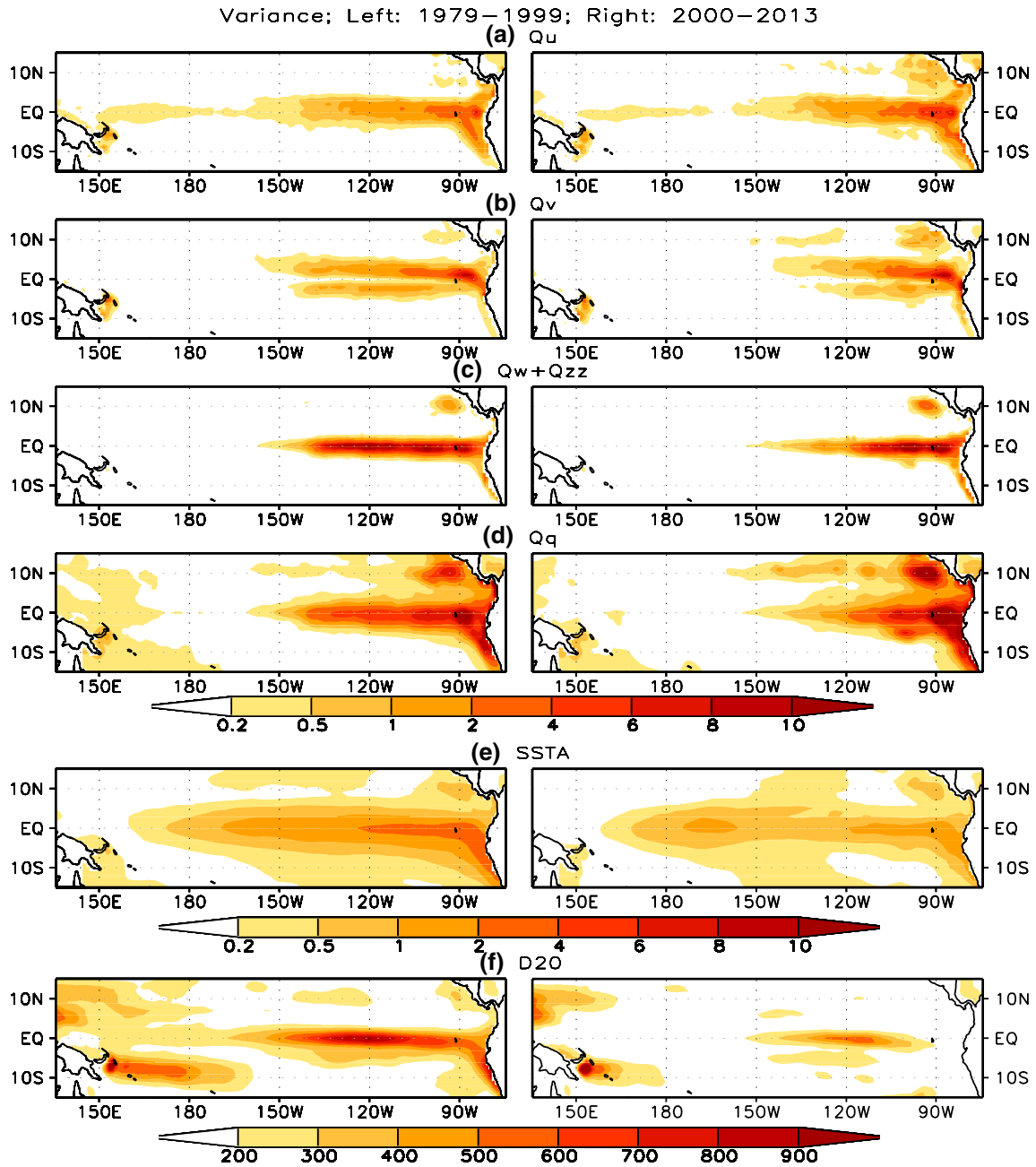

Fig. 11 Variances of **a** Q_u, **b** Q_v, **c** Q_w+Q_{zz}, **d** Q_q, **e** SSTA, and **f** D20 anomaly (*left panels* for Jan 1979–Dec 1999 and *right panels* for Jan 2000–Dec 2013). The unit is $(°C/month)^2$ for (**a**–**d**), $(°C)^2$ for (**e**), and m^2 for (**f**)

in GODAS (Huang et al. 2010; Zhu et al. 2012) might be also a factor affecting the detailed spatial structures of these leading modes and their association with ENSO at some extent. The qualitative similarity between the tendency term and the sum of all resolved physical terms suggest that the residual term ["R" in Eq. (1)] is secondary in explaining the patterns associated with these two modes. If the residual terms are approximated by the absolute difference between SST tendency and total forcing (not shown), it is noted that they are relatively small, suggesting that they play a relatively minor role in the equatorial Pacific. One approach to further examine the reliability of ocean heat budget calculation may be through comparison of multi-ocean re-analyses.

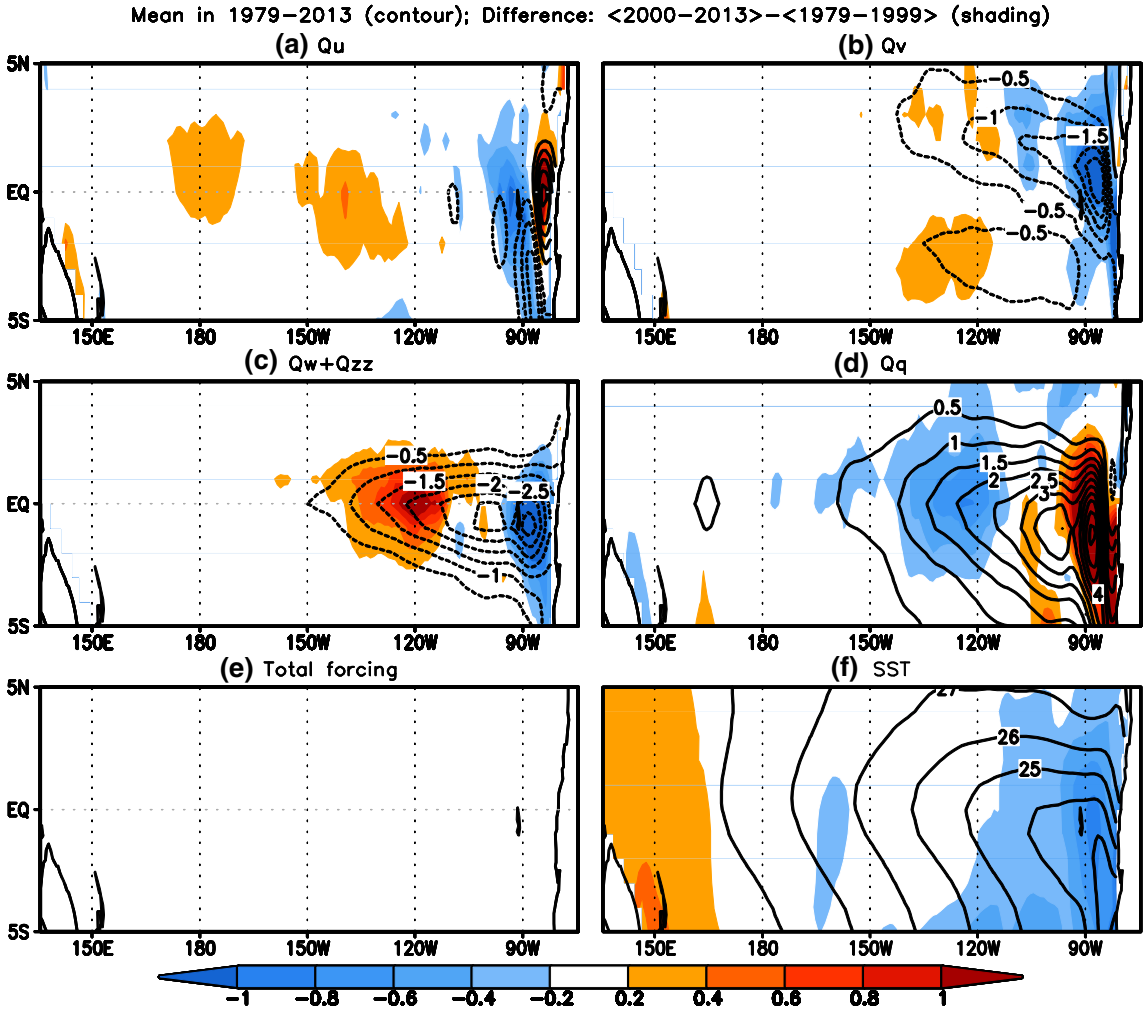

Fig. 12 Mean averaged in Jan 1979–Dec 2013 (*contour*) and the difference between Jan 2000–2013 and Jan 1979–Dec 1999 (*shading*) of **a** Q_u, **b** Q_v, **c** Q_w+Q_{zz}, **d** Q_q, **e** total forcing terms, and **f** SST. The unit is °C/month for (**a**–**e**), and °C for (**f**). The contour interval is 0.5 °C/month in (**a**–**e**), and 1 °C in (**f**). Zero *contour line* is not shown

Acknowledgments We appreciated the insight comments and suggestions from two reviewers, which significantly improve the paper. We discussed with Prof. Fei-Fei Jin during early stage of this work. Bohua Huang is supported by grants from NSF (ATM-0830068), NOAA (NA09OAR4310058), and NASA (NNX09AN50G). The procedure of the heat budget calculation used in this work was developed by Dr. Boyin Huang and is maintained by Dr. C. Wen. The scientific results and conclusions, as well as any view or opinions expressed herein, are those of the author(s) and do not necessarily reflect the views of NWS, NOAA, or the Department of Commerce.

References

Barnston AG, Chelliah M, Goldenberg SB (1997) Documentation of a highly ENSO-related SST region in the equatorial Pacific. Atmos Ocean 35:367–383

Battisti DS, Hirst AC (1989) Interannual variability in a tropical atmosphere-ocean model: influence of the basic state, ocean geometry and nonlinearity. J Atmos Sci 46:1687–1712

Bay T, Dommenget D (2014) Comparing the spatial structure of variability in two datasets against each other on the basis of EOF-modes. Clim Dyn 42:1631–1648

Behringer DW (2005) The global ocean data assimilation system (GODAS) at NCEP, 11th Symposium on Integrated Observing and Assimilation Systems for the Atmosphere, Oceans, and Land Surface (IOAS-AOLS), San Antonio, TX, Amer. Meteor. Soc., 3.3 [Available online at https://ams.confex.com/ams/87ANNUAL/webprogram/11IOAS.html]

Behringer DW, Xue Y (2004) Evaluation of the global ocean data assimilation system at NCEP: the Pacific Ocean. Preprints, Eighth Symp. on Integrated Observing and Assimilation Systems for Atmosphere, Oceans, and Land Surface, Seattle, WA, Amer. Meteor. Soc., 2.3 [Available online at http://ams.confex.com/ams/84Annual/techprogram/paper_70720.htm]

Bjerknes J (1969) Atmospheric teleconnections from the equatorial Pacific. Mon Weather Rev 97:163–172

Clarke AJ (2010) Analytical theory for the quasi-steady and low-frequency equatorial ocean response to wind forcing: the 'tilt' and 'warm water volume' modes. J Phys Ocean 40(1):121–137

Dommenget D, Latif M (2002) A cautionary note on the interpretation of EOFs. J Climate 15:216–225

Glantz MH (2000) Currents of change: impacts of El Niño and La Niña on climate and society. Cambridge University Press, Cambridge, UK, p 266. ISBN 052178672X

Hu Z-Z, Nitta T (1996) Wavelet analysis of summer rainfall over North China and India and SOI using 1891–1992 data. J Meteorol Soc Jpn 74(6):833–844

Hu Z-Z, Kumar A, Jha B, Wang W, Huang B, Huang B (2012) An analysis of warm pool and cold tongue El Niños: air-sea coupling processes, global influences, and recent trends. Climate Dyn 38(9–10):2017–2035. doi:10.1007/s00382-011-1224-9

Hu Z-Z, Kumar A, Ren H-L, Wang H, L'Heureux M, Jin F-F (2013a) Weakened interannual variability in the tropical Pacific Ocean since 2000. J Climate 26(8):2601–2613. doi:10.1175/JCLI-D-12-00265.1

Hu Z-Z, Kumar A, Huang B, Zhu J (2013b) Leading modes of upper ocean temperature interannual variability along the equatorial Atlantic Ocean in NCEP GODAS. J Climate 26(13):4649–4663. doi:10.1175/JCLI-D-12-00629.1

Huang B, Schneider EK (1995) The response of an ocean general circulation model to surface wind stress produced by an atmospheric general circulation model. Mon Weather Rev 123:3059–3085

Huang B, Xue Y, Zhang D, Kumar A, McPhaden MJ (2010) The NCEP GODAS ocean analysis of the tropical Pacific mixed layer heat budget on seasonal to interannual time scales. J Climate 23:4901–4925

Huang B, Xue Y, Wang H, Wang W, Kumar A (2012) Mixed layer heat budget of the El Niño in NCEP climate forecast system. Climate Dyn 39(1–2):365–381. doi:10.1007/s00382-011-1111-4

Jin F-F (1997a) An equatorial ocean recharge paradigm for ENSO. Part I: conceptual model. J Atmos Sci 54:811–829

Jin F-F (1997b) An equatorial ocean recharge paradigm for ENSO. Part II: a stripped-down coupled model. J Atmos Sci 54:830–847

Kanamitsu M et al (2002) NCEP-DOE AMIP-II Reanalysis (R-2). Bull Am Met Soc 83:1631–1643

Kang I-S, An S-I, Jin F-F (2001) A systematic approximation of the SST anomaly equation for ENSO. J Meteorol Soc Jpn 79:1–10

Kao H-Y, Yu J-Y (2009) Contrasting eastern-Pacific and central-Pacific types of ENSO. J Climate 22:615–632

Kug J-S, Jin F-F, An S-I (2009) Two types of El Niño events: cold tongue El Niño and warm pool El Niño. J Climate 22:1499–1515. doi:10.1175/2008JCLI2624.1

Kumar A, Hu Z-Z (2014) Interannual and interdecadal variability of ocean temperature along the equatorial Pacific in conjunction with ENSO. Climate Dyn 42(5–6):1243–1258. doi:10.1007/s00382-013-1721-0

Lau N-C, Philander SGH, Nath MJ (1992) Simulation of ENSO-like phenomena with a low-resolution coupled GCM of the global ocean and atmosphere. J Climate 5(4):284–307

Lee T, McPhaden MJ (2010) Increasing intensity of El Niño in the central equatorial Pacific. Geophys Res Lett 37:L14603. doi:10.1029/2010GL044007

McPhaden MJ (2012) A 21st century shift in the relationship between ENSO SST and warm water volume anomalies. Geophys Res Lett 39:L09706. doi:10.1029/2012GL051826

Meinen CS, McPhaden MJ (2000) Observations of warm water volume changes in the equatorial Pacific and their relationship to El Niño and La Niña. J Climate 13:3551–3559

National Research Council (2010) Assessment of Intraseasonal to Interannual Climate Prediction and Predictability. The National Academies Press, Washington, p 192. ISBN 0-309-15183-X

North GR, Bell TL, Cahalan RF, Moeng FJ (1982) Sampling errors in the estimation of empirical orthogonal functions. Mon Weather Rev 110:699–706

Picaut J, Masia F, du Penhoat Y (1997) An advective-reflective conceptual model for the oscillatory nature of the ENSO. Science 277:663–666

Rasmusson EM, Carpenter TH (1982) Variation in tropical sea surface temperature and surface wind fields associated with Southern Oscillation/El Niño. Mon Weather Rev 110:354–384

Reynolds RW, Rayner NA, Smith TM, Stokes DC, Wang W (2002) An improved in situ and satellite SST analysis for climate. J Climate 15:1609–1625

Sarachik ES, Cane MA (2010) The El Niño-Southern Oscillation Phenomenon. Cambridge University Press, London **384 pp**

Schopf PS, Suarez MJ (1987) Vacillations in a coupled ocean-atmosphere model. J Atmos Sci 45:549–566

Walker GT (1923) Correlations in seasonal variations of weather, VIII. A preliminary study of world weather I. Mem India Meteorol Dep 23:75–131

Wang C (2001) A unified oscillator model for the El Niño-Southern Oscillation. J Climate 14:98–115

Wang W, Chen M, Kumar A (2010) An assessment of the CFS real-time seasonal forecasts. Weather Forecast 25:950–969

Wen C, Kumar A, Xue Y, McPhaden MJ (2014) Changes in tropical pacific thermocline depth and their relationship to ENSO after 1999. J Climate 27:7230–7249

Wyrtki K (1975) E1 Niño-the dynamic response of the equatorial Pacific Ocean to atmospheric forcing. J Phys Ocean 5:572–584

Wyrtki K (1985) Water displacements in the Pacific and the genesis of El Niño cycles. J Geophys Res 90(C4):7129–7132

Xiang B, Wang B, Li T (2013) A new paradigm for the predominance of standing Central Pacific warming after the late 1990s. Climate Dyn 41(2):327–340. doi:10.1007/s00382-012-1427-8

Yeh S, Kug J, Dewitte B, Kwon M, Kirtman BP, Jin F-F (2009) El Niño in a changing climate. Nature 461(7263):511–514

Zebiak SE, Cane MA (1987) A model El Niño/Southern Oscillation. Mon Wea Rev 115:2262–2278

Zhang R-H, Levitus S (1996) Structure and evolution of interannual variability of the tropical Pacific upper ocean temperature. J Geophys Res 101:20501–20524

Zhang Q, Kumar A, Xue Y, Wang W, Jin F-F (2007) Analysis of ENSO cycle in NCEP coupled forecast model. J Climate 20:1265–1284

Zhu J, Huang B, Balmased MA (2012) An ensemble estimation of the variability of upper-ocean heat content over the tropical Atlantic Ocean with multi-ocean reanalysis products. Climate Dyn 39(3–4):1001–1020. doi:10.1007/s00382-011-1189-8